Indian Journal of Chemical Technology
Vol. 33, May 2026, pp. 413-426
DOI: 10.56042/ijct.v33i3.17621

Effect of vinyl resin addition on the adhesion strength of anti-corrosion zinc-rich epoxy coating on A283 steel

Amal Meghalet[1], Amel Halimi[2], Sofia Benamirouche[3], Larbi Hemmouche[1]*, Yazid Touazi[3] & Mohamed Daia Dine Boudiaf[1]

[1]Laboratoire Génie des Matériaux, Ecole Militaire Polytechnique, BP17 Bordj El-Bahri, 16046 Algiers, Algeria

[2] Ecole Supérieure des Techniques de l'Aéronautique, Alger

[3]Laboratoire Electrochimie et Corrosion, Ecole Militaire Polytechnique, BP17 Bordj El-Bahri, 16046 Algiers, Algeria

*E-mail: l.hemmouche@gmail.com

Received 8 March 2025; accepted 2 April 2026

The objective of this study is to improve the adhesive properties of anticorrosion zinc-rich coatings. This was achieved by introducing modifications, specifically by incorporating vinyl resin into the base formulation which consisting of epoxy resin and zinc powder. The efficacy of the newly modified coating (ZRC-M) was assessed in comparison to a commercially available zinc-rich epoxy coating (ZRC-C). Coatings with both formulations (ZRC-C and ZRC-M) were applied to the carbon steel panels. The main methods employed to investigate the corrosion protection efficacy and adhesion of the two variants of zinc-rich epoxy coatings included DC linear polarization, electrochemical impedance spectroscopy (EIS), salt spray exposure, and the pull-off test. The results revealed that the adhesion improved in ZRC-M compared to ZRC-C, while maintaining an equivalent level of anticorrosion protection. With the decrease in coating density and viscosity, the electrochemical impedance spectroscopy results obtained at the open circuit corrosion potential indicated that the addition of vinyl resin enhanced the effective zinc content and the barrier effect of the coating after a forty-day immersion period, attributable to the reduce of electrical conductivity of the coating.

Keywords: Adhesion, Anticorrosion, A283steel, Coating, Corrosion, Vinyl resin, Zinc-rich epoxy coating

Introduction

Epoxy resin systems are widely used in construction and industry due to the excellent combination of mechanical properties, chemical stability, adhesion, corrosion and wear resistance to most metals and alloys[1,2]. The nature of the bond between the steel substrate and the epoxy coating is primarily in the form of physical bonds through mechanical interlocks and/or chemical bonds that are unstable under wet conditions. Therefore, for good adhesion, a covalent bond must be formed between the steel substrate and the epoxy coating[3,4]. Zinc-rich epoxy coatings (ZRC) are commonly used as primers and have excellent corrosion resistance[5,6]. This is very important for corrosion protection of steel in atmospheric and aqueous environments[7]. The protection mechanism of ZRC coating corresponds to a combination of cathodic protection and barrier effects[8]. Cathodic protection of substrates is achieved by using zinc powder as anodic sacrificial filler in ZRC coatings that have a corrosion potential more negative than the substrate to be protected. Various efforts are being made to improve the corrosion resistance of ZRC coatings which provide good sacrificial protection early in their life cycle. However, at later stages, ZnO/ZnOH is generated, resulting in reduced metal particle contact. In fact, zinc corrosion products can fill the pores of the coating, thereby shortening the cathodic protection time[9,10]. In this case, the coating exhibits more barrier properties than cathodic protection. The sacrificial protection of ZRC depends on many factors, mainly morphology and percentage of zinc particles[11]. Schaefer and Miszczyk[5] investigated the cathodic protection properties of ZRC by substituting nanoparticles of zinc for a small fraction of micro zinc powder, which remaining under the cathodic protection for the longest time. Before this many research substrates high percentage of particle of zinc (more than 60%) to insure a good electrical contact between zinc and steel substrate[6,12].

Numerous studies have been reported in the literature to develop ZRC with improved barrier performance and extended cathodic protection property by partial substitution of zinc particles with electrically conductive and nonconductive fillers such as polyaniline[12-14], carbon nanotubes[14,15], aluminum pigments, micaceous iron

oxide[16,17], ZnO[18], Alumina[19], and nano-clay[20]. Recently, a novel method is developed consist to using graphene nanosheets with its impermeable nature to enhance both barrier and percolation properties of ZRC[21,22]. Furthermore, the impermeable barrier role was reinforced by including prepared reduced graphene oxide nanosheets into the polymer matrix[23]. In addition, the electrical connection between the zinc particles and steel substrate improve the electrical conductivity of ZRC by using the reduced graphene oxide nanosheets[24-27]. In the same optic, a modified graphene oxide by sulfonated multiwall carbon nanotubes[28] and by MXene (Ti_3C_2)[29], increases the shielding effect and the electrical connection between Zn particles and metal substrates, which improves the corrosion resistance. Sacrificial properties of ZRC can be extended by surface modification of zinc particles to slow down its dissolution rate, thus suppressing its electrochemical reactivity while maintaining the electrical percolation[30,31].

Surface modification method, involves treating micro zinc particles (lamellar or spherical) with organic or inorganic (such as silicates, phosphates, and dichromate) chemicals possessing, provide good corrosion inhibition ability[32]. The Diglycidyl ether of Bisphenol A epoxy resin is the most frequently used as a binder for ZRC due to their processing simplicity, excellent chemical resistance, high cross-link density, important adhesive strength and high compatibility with different classes of coats[33,34]. Since epoxy resin doesn't have good electrical conductivity, a high percentage of zinc particles (80- 90 wt. %) are needed to ensure electrical conductivity between zinc particles and metal substrate for galvanic action[35].Vinyl resins are used as primers in industrial coatings where the repaint interval exceeds 20 years[36]. They are used in coatings for blind strips and bottle caps where extreme flexibility and extrudability are required. They are also used in heavy duty and marine coatings where properties such as toughness, elasticity and water resistance are critical, and as thick coats on architectural siding coil coating tapes. Because of these properties, vinyl resin is gaining scientist's attention for preparing anti-corrosion coatings[37]. Epoxy-vinyl resins exhibit chemical inertness in water, suggesting their potential as effective barriers against corrosion in metallic structures immersed in aqueous environments[38]. Renowned for durability, epoxy-vinyl paint excels at forming strong bonds that enhance adhesion, making it particularly suited for protective applications[39-42].

This work examines the corrosion protection of A283 steel in aggressive environments through the application of a commercial zinc-rich coating (ZRC-C). The contribution of this research resides in the incorporation of vinylic resin into the ZRC-C, in order to analyze the performance of the interface between the organic coating and the steel substrate regarding corrosion resistance and adhesion strength.

Experimental Section

Painting surface and paint

The material investigated in this study is A283 C steel. The chemical composition and the mechanical property of this tested steel are given in Table 1.

Two epoxy zinc-rich paint formulations were prepared at the National Company of Paints (ENAP-Algiers). The first, labeled ZRC-C, contained 80% zinc particles (supplied by Umicore Zinc Powder - Belgium) and 12% Epikote 1001 epoxy resin(based on bisphenol-A in a xylen solution having the solid content and density of 74-76 wt% and 1.08 g/cm³, respectively). The second, designated ZRC-M used the same zinc particles but with a modified resin blend of 6% Epikote 1001 and 2.22% Laroflex 45 (BASF Resin, Allemagne) vinyl resin. The zinc dust used in this study exhibited an average particle size of 4.4 μm, oil absorption of 6.45 g/100 g pigment, and a density of 7.14 g/cm³.

The coating formulations were supplemented with 0.2 wt% of NUOSPERSE 657 pigment dispersing agent and 6.8 wt% of Argil arnophil treated rheological modifier. These mixtures were subsequently subjected to 20 min of mechanical mixing at 1000 rpm. Finally, a stoichiometric quantity of a polyamidoamine curing agent (solid content of 69-71%) was used.

Two types zinc-rich coatings were prepared using Zn pigment at different volume concentrations (PVCs) with 60.40 % for ZRC-M and 52.38 % for ZRC-C according to Eq. 1. Subsequently, the critical pigment volume

Table1 — Chemical composition and mechanical property of A 283 grade C steel

	Chemical composition (wt. %)						Mechanical property		
	C	Mn	Si	P	S	Cu	Re (MPa)	A %	Rm (MPa)
Norm max (ASME II)	0.14	0.9	0.04	0.035	0.4	0.2	Min 185	28	345-485
A283 C steel	0,12	0.68	0.17	0.013	0.004	0.04	186	26	425

concentration (CPVC) values were calculated through the Eq. 2 with 70.10% for and 83.43% ZRC-C:

$$PVC = \frac{V_1}{V_1 + V_2} \quad \ldots (1)$$

$$CPVC = \frac{1}{1 + \frac{OxD}{\rho}} \quad \ldots (2)$$

Where V_1 is the volume of the zinc dust, V_2 is the volume of the epoxy resin, O is the oil absorption and D is the density of the zinc dust. For a typical zinc-rich coating with appropriate sacrificial properties, the ratio of PVC to CPVC is greater than one[17].

Coating process

The samples dimensions used in the present work were 43 mm × 45 mm × 13 mm. The specimens were subjected to sand blasting in accordance with Sa 2.5 standards outlined in both ISO 12944 and ISO 8501. Subsequent surface roughness measurements using a dedicated instrument yielded (TESA-rugosurf 90-G) an average Ra value of approximately 6.2 µm for all panels. ZRC-C and ZRC-M were applied to the substrate using a paint applicator. After curing, the coating film thickness ranged from 40 to 60 µm, as measured by Exacto Elektrophysik for both adhesion and electrochemical panel tests.

Immersion

The samples were submerged in a 3.5% NaCl solution at room temperature. Subsequently, at predetermined intervals of 2, 6, 10, 14, 24, 27, 34, and 40 days, they were meticulously extracted from the solution for thorough examination, including comprehensive analysis of mechanical, electrochemical, and surface properties.

Characterization techniques

Paint properties

In this study, viscosity, density, FTIR and conductivity test were used for characterization of the two types of paints. The viscosity and density were rigorously measured at 25°C according to established international standards. Employing a Brookfield viscometer (M6 spindle) calibrated to ISO 2884-1 and an ALCOMETER-tested machine ensured accurate viscosity determination at 5 rpm spindle speed. Additionally, the ZRC coating's density was precisely determined at 25°C based on the pycnometer's mass, adhering to ISO 2811-1 guidelines.

Spectral analysis of ZRCs paints was performed by means of a Perkin Elmer Fourier transform infrared spectroscopy (FTIR) spectrometer by the attenuation total reflection (ATR) method. Spectra were recorded at 2 cm^{-1} resolution for 32 scans and the scanning range was 4000 – 400 cm^{-1}.The resistivity and conductivity of the coatings were determined using a Jandel RM 3000 double electric four-point probe tester. The average probe spacing was maintained at 1 mm, and the current range was kept constant. The coating thickness was measured to be 4.5 mm and 6.1 mm after the paint molding process.

Coating characterization and measurement

Surface morphology analysis

The Zn particles distributions in the zinc-rich coatings were observed by a ZEISS type scanning electron microscope (SEM). The surface morphology of the zinc-rich coatings was also examined by SEM after 40 days of immersion in 3.5 % NaCl. Energy dispersive X-ray spectrometry (EDS) was employed for analyzing the corresponding elemental compositions.

Pull-off tests

In order to evaluate the adhesion strength of the epoxy coating following ASTM D 4541 Standard, pull-off tests were performed. Using two-part quick epoxy adhesive A/B (ALTECO), dollies with a diameter of 20 mm were fixed onto the epoxy coating. The samples were then left to cure fully at room temperature for more than 24 h to ensure complete adhesive bonding. Subsequently, the dollies were subjected to control pulling at a rate of 10 mm/min perpendicular to the specimen surface until the epoxy coating detached from the substrate.

Corrosion characterization

Electrochemical measurements were conducted in Ametek PARSTAT 4000 electrochemical workstation combined with corrosion program (Versa Studio). The working electrode for electrochemical impedance spectroscopy was deposed to expose a circular surface area of 706 mm^2 to the electrolyte (the test cell was replaced after 14 days of immersion). The testing setup comprised the coated sample serving as the working electrode, a saturated calomel electrode (SCE) utilized as the reference electrode, and a platinum counter electrode with a 10 mm^2 area. These electrodes were employed for conducting measurements involving open circuit potential (OCP), electrochemical impedance spectroscopy (EIS), and DC polarization technique. The potentiodynamic current – potential curves were recorded by changing the electrode potential automatically from -150 to

+250 mV with a scan rate 0.33 $mV^{-1}s$. The EIS was collected at the open circuit potential with the frequency ranging from 105 Hz to 0.01 Hz and at amplitude sinusoidal voltage of ±10 mV. The recorded spectra were analyzed as Nyquist and Bode diagrams. They were fitted using a homemade simplex procedure. The impedance at 10 mHz was compared in this investigation.

The salt spray test was carried out in a salt spray cabin DCTC 600 according to ASTM B117. The test was done on 35 mm x 35 mm area of the samples having the same coating thickness (100 µm). To isolate the designated area, the remaining surface of the coating was masked with silicone. Subsequently, a 5.0 wt.% NaCl solution was atomized and continuously sprayed onto the samples at a temperature approximately around 40°C. The relative humidity was maintained at a collection rate of at least 52%.

Results and Discussion

Paint properties

The physical and chemical properties of ZRC-C and ZRC-M were investigated through viscosity, density, conductivity, and FTIR analyses. Table 2 displays the viscosity and density measurements of the paints. The densities of ZRC-C and ZRC-M were comparable, with a slight decrease observed for ZRC-M. Additionally, the results indicate the significant influence of low-viscosity vinyl resin (0.04 Pa.s) on the dynamic viscosity of the coatings. Furthermore, ZRC-M demonstrates notably lower viscosity compared to ZRC-C for the same zinc particle content.

The FTIR spectra in Fig. 1 (a) reveal the specific functional groups present in each sample, providing insight into their chemical structure characteristics. Both spectra exhibit a similar overall profile, characterized by more than five absorption peaks indicative of complex molecular structures. Moreover, the spectra obtained for ZRC-C and ZRC-M exhibited absorption peaks at 2900 cm^{-1}, which are attributed to linear aliphatic compounds, and a characteristic doublet at 756 and 824 cm^{-1}, associated with aromatic compounds (single strong band at 750 cm^{-1} for ortho and 830 cm^{-1} for para, as reported[39]).

Notably, these include peaks at 1034 cm^{-1}, 3408 cm^{-1}, and 1240 cm^{-1}, which correspond to the stretching vibrations of the epoxide C–O–C bond, the hydroxyl O–H bond, and the C–O bond, respectively. As shown in Fig. 1 (b), the absorption peak at 964 cm^{-1} suggests the presence of vinyl-related compounds, particularly trans unsaturated vinyl (CH=CH). This peak is dispersed within the FTIR spectra of the modified zinc-rich coating, and new bonds emerge at 1720 cm^{-1}, attributed to carboxyl (C=O) groups.

Table 3 presents the measured values of resistivity and conductivity for ZRC-C and ZRC-M. It has been observed that ZRC-C demonstrates higher electrical

Table 2 — Viscosity and density results

	ZRC-C	ZRC-M
Density	3.18 ± 0.05	3.125 ± 0.05
Viscosity (Poise)	1240 Po ± 60	1050 Po ±60

Table 3 — Resistivity and conductivity of the coatings

	ZRC-C		ZRC-M	
Current	Conductivity S/m	Resistivity Ω.m	Conductivity S/m	Resistivity Ω.m
10 nA	$14{,}2\ 10^{+07}$	$70{,}4\ 10^{-08}$	$3{,}02\ 10^{+07}$	$3{,}31\ 10^{-08}$
10 µA	$13{,}6\ 10^{+04}$	$73{,}5\ 10^{-05}$	$2{,}75\ 10^{+04}$	$3{,}63\ 10^{-05}$
10 mA	$13{,}8\ 10^{+01}$	$72{,}5\ 10^{-02}$	$2{,}65\ 10^{+01}$	$3{,}77\ 10^{-02}$

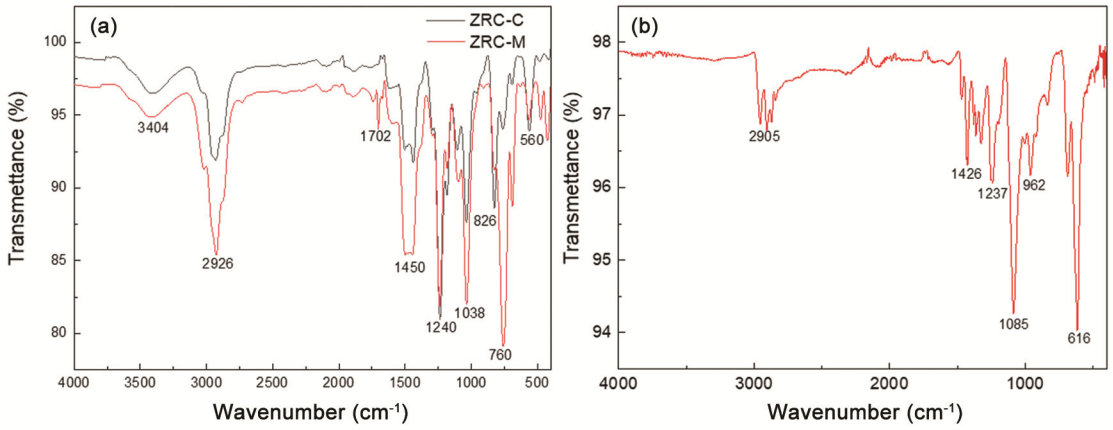

Fig. 1 — Fourier transform infrared spectra of (a) ZRC-C & ZRC-M and (b) vinyl resin

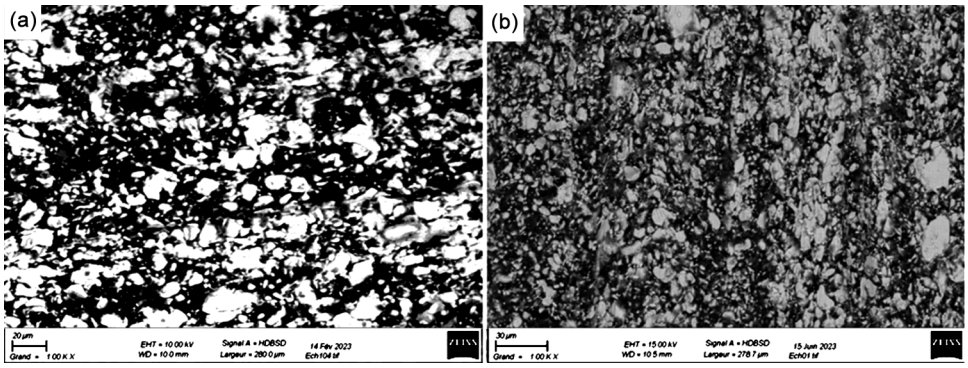

Fig. 2 — SEM micrographs of (a) ZRC-C and (b) ZRC-M

conductivity than the modified ZRC-M coating. The variance in conductivity can be attributed to the difference in the nature of the resin used. Indeed, the conductivity of epoxy is approximately 150 S/cm[ref.43], while that of vinyl is around 40 S/cm for the same percentage of zinc (conductivity ≈1.7×10^7 S/m). Therefore, this attributed to the "barrier effect" caused by the addition of vinyl, which hinders the flow of electrons within the coating, thus impeding the transmission of electric charges.

Coating characterization and measurement

Morphology of the coatings

Fig. 2 shows SEM images of ZRC-C and ZRC-M coatings. The surface of the sample appears very smooth, and there are no spherical zinc particles visible on the surface of the coating. This indicates uneven dispersion of the zinc powder. Indeed, the two coatings have almost the same sedimentation rate of ZRC-C and ZRC-M are respectively 2.42 and 2.37. These values are estimated by Stockes settlement formula[40]: give as follows.

$$W = \frac{g\,x\,d^2\,x(\rho_d - \rho)}{18\,x\,\mu} \quad \ldots (3)$$

Where, W is sedimentation rate; g is acceleration of gravity; d is the particle size of zinc powder; ρ_d is the density of zinc; ρ is the density of resin and μ is the viscosity of resin.

Pull-off test

The effects of vinyl modification on the adhesion properties of ZRC coatings were evaluated using pull-off tests. According to the NF EN ISO 12944-6 standard, epoxy coatings have to exhibit an adhesion value of at least 2.5 MPa after immersion[44].

Figs 3 and 4 give results of Pull-off measurements of the epoxy coatings applied on the surface of steel.

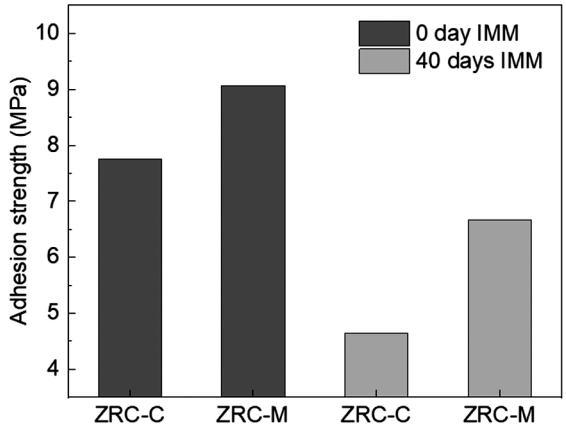

Fig. 3 — Adhesion strength for ZRE-C, ZRE-M before and after immersion time

The results in Fig. 3 demonstrate that both ZRC-C and ZRC-M coatings respect NF EN ISO 12944-6 condition; all results are more than 4.5 MPa. A noticeable decline in adhesion strength is observed before and after immersion in a corrosive environment. This is attributed to the degradation of the epoxy resin matrix and the weakening of the interfacial bond between the coating and the steel substrate.

Coating adhesion strength is primarily governed by two factors: (1) Cohesion: The internal strength of the coating itself, and (2) adhesion: The interfacial bond between the coating and the substrate[43]. From Fig. 4, it can be observed that there is a greater occurrence of adhesive failure on the surface of ZRC-M before immersion compared to ZRC-C. This indicates that the incorporation of vinyl into the ZRC-C enhances both aspects of adhesion strength. The increased surface free energy and wettability give stronger adhesion between the coating and the substrate, while the enhanced crosslinking density of the vinyl-modified epoxy resin improves the cohesion of the

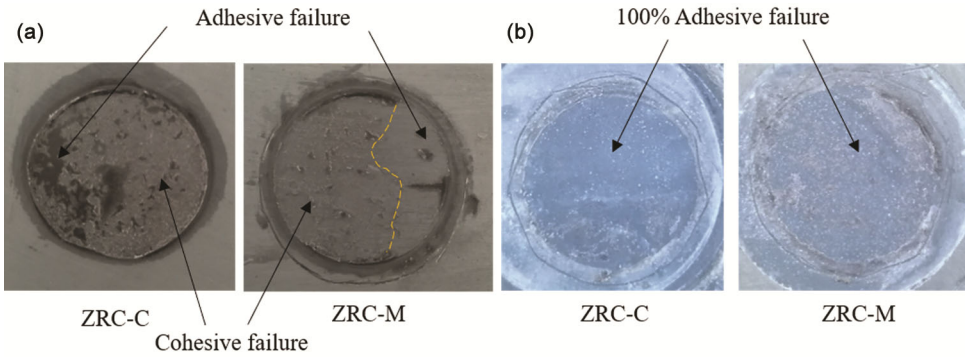

Fig. 4 — Visual performance of pull off tests: (a) before and (b) after immersion

coating itself[28]. After an immersion period of 40 days, both samples exhibited no cohesive failure. However, the bond strength varied between samples, indicating the impact of particle dissolution into the resin. The decrease in pull-off force is attributed to the formation of corrosion products. These products effectively fill the porous surfaces of both primer layers, thereby reducing their adhesion.

Corrosion characterization

OCP measurements

The open circuit potential (OCP) is a crucial parameter for assessing whether ZRC effectively protects the underlying metal substrate through cathodic sacrificial action. Variations in OCP (vs. SCE) for ZRC-C and ZRC-M coatings at different immersion times are given in Fig. 5. A ZRC is considered effective for cathodic protection if its potential falls within the range from -1.143 to -0.8 V/SCE[44]. It is observed that both ZRC-M with potentials ranging from -1.08 to -0.88 V/SCE and ZRC-C with potentials ranging from -1.075 to -0.96 V/SCE maintain their OCP within the optimal range for cathodic protection, indicating their effectiveness in providing adequate corrosion protection.

Until the 14th day of immersion, both coatings showed comparable behaviour, where the ZRC-C coating displayed a more negative corrosion potential than the ZRC-M coating. This disparity might imply that ZRC-C offers superior cathodic protection efficiency over ZRC-M. However, beyond this period, the ZRC-C coating exhibited significantly more negative corrosion potential values compared to the initial period, indicating an improved ability to inhibit corrosion-causing anodic reactions. Therefore, the increase in the potential of ZRC-M corresponds to a decrease in cathodic protection, which is caused by the precipitation of zinc corrosion products around the

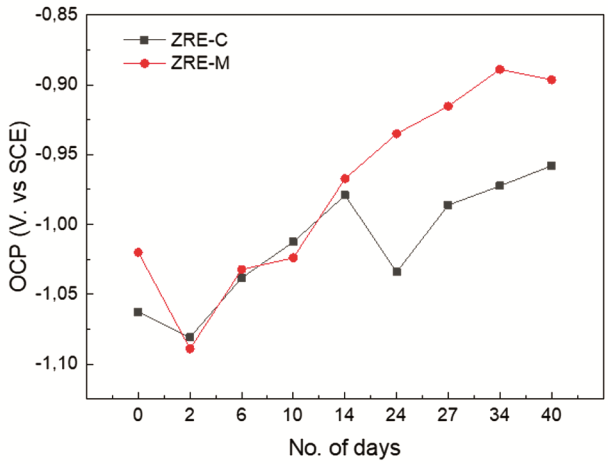

Fig. 5 — Variation of Open Circuit Potential (OCP) vs immersion time of ZRCs

zinc particles. Consequently, leads to a reduction in electrical contact between zinc particles and the galvanic connection between zinc and the steel substrate. Although the zinc content in both coatings was similar, the discrepancy in corrosion potential changes is attributed to the vinyl formulation, which can decrease the surface porosity, thus limiting the penetration of electrolytes. Therefore, these observations indicate an improvement in the barrier effect of the ZRC-M (which confirms the conductivity results).

EIS measurements

Graphical analysis with immersion time

The corrosion protection efficacy of ZRC-M was investigated using Electrochemical Impedance Spectroscopy (EIS) with ZSimpWin software. Experiments were conducted under varying immersion times in 3.5 % NaCl solution, and the resulting Bode and Nyquist plots are presented in Fig. 6.

From the Nyquist plot (Fig. 6 (a1, b1)) of each coating, two distinct levels can be identified during

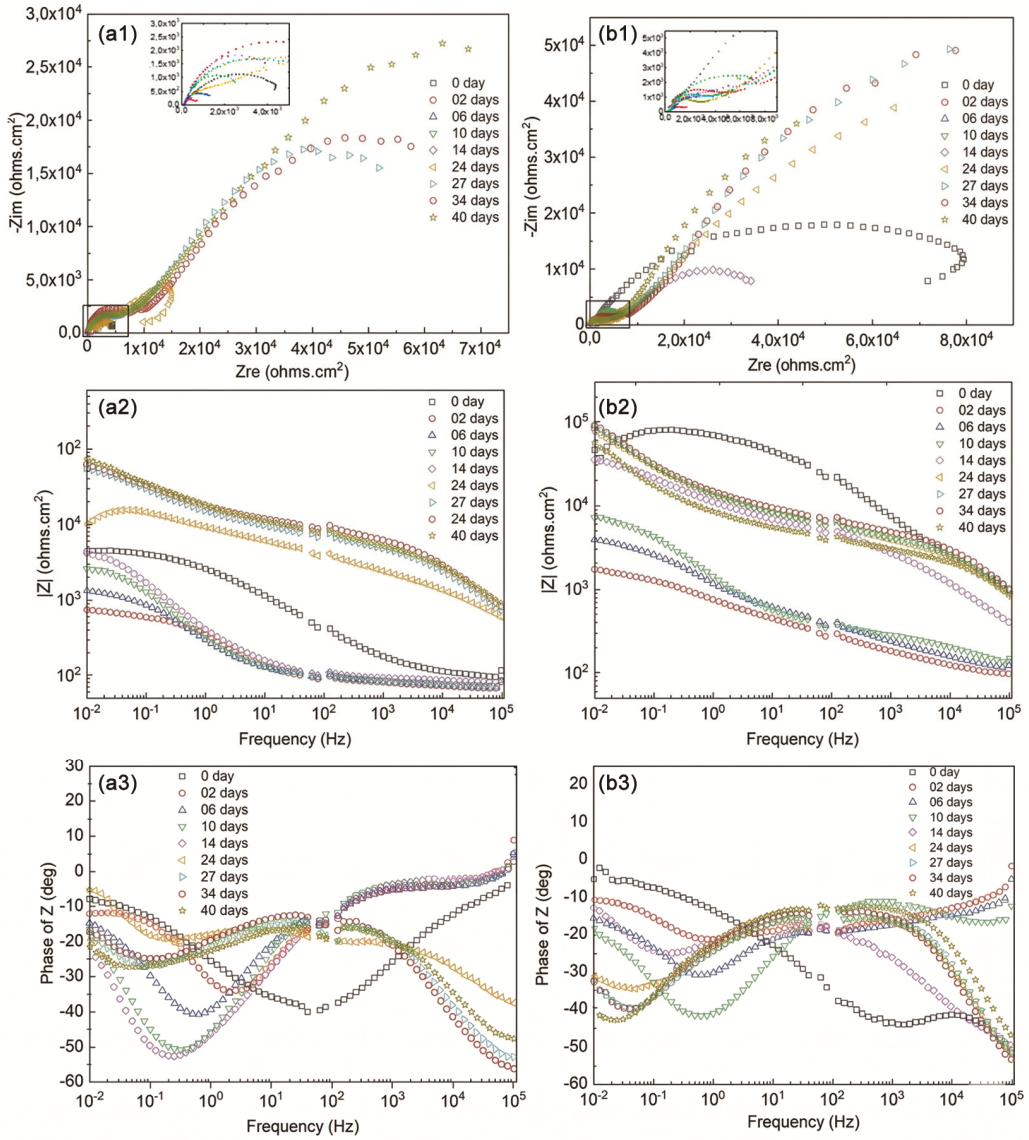

Fig. 6 — Nyquist and Bode diagrams of the (a1, a2, a3) ZRC-C, (b1, b2, b3) ZRC-M, samples after 0.5 h, 02, 06, 10, 14, 24, 27, 34 and 40 days immersion in 3.5 wt.% NaCl sol

the immersion procedure. Initially, at the first level, only one capacitive arc is observed at the beginning of immersion, representing the water uptake process in the coating.

From the Nyquist plot (Fig. 6 (a1, b1)) of each coating, two distinct levels can be identified during the immersion procedure. Initially, at the first level, only one capacitive arc is observed at the beginning of immersion, representing the water uptake process in the coating. At the second level after two days of immersion, curves exhibit two-time constants, reflecting the initiation of a gradual permeation of electrolyte through the zinc-rich coating with a high zinc content (70-90% zinc dust, in our case 80%).

The first arc at high frequency represents the impedance and capacitance of the coating, corresponding to the charge transfer associated with the ionic double layer capacitance and the activation of zinc metal to provide cathodic protection to the substrate. The low-frequency arc or semicircle indicates diffusion processes of finite layer thickness or the zinc dissolution reaction, primarily related to oxygen reduction. This corresponds to the characteristic Warburg impedance observed in EIS curves.

Up to 10 days, the low-frequency arc or semicircle progressively contracts more for ZRC-M with little development on the capacitive arc at high frequency.

This is attributed to the formation of a dense layer of zinc corrosion products that effectively seals microscopic defects in the outer coating layer, thus hindering the mass transfer of reactants and products. At the same time, we observe lower progressivity on impedance at the low frequency, suggesting a stronger charge transfer effect in ZRC-C.

The phase angle plots (Fig. 6 (a_3,b_3) confirm previous findings. Initially, at low frequency, a single peak is evident at the start of immersion, whereas at the conclusion of immersion, only two peaks are observed at low and high frequencies. This discrepancy is primarily attributed to the distinct percolation structures of the coating layers.

The impedance modulus |Z| at the lowest frequency (0.01 Hz) in the Bode diagram serves as an indicator of the coating's impermeability[45]. Initially, the impedance modulus of both samples exhibits a decrease with immersion time, reflecting the gradual infiltration of the electrolyte solution into the coating, as depicted in Fig. 7. After 14 days of immersion in the electrolyte solution, the ZRC-C sample's impedance modulus reaches $4.35 \times 10^3 \Omega \cdot cm^2$, while it decreases to $0.7 \times 10^3 \Omega \cdot cm^2$ and $4.1 \times 10^3 \Omega \cdot cm^2$ after soaking for 02 days and 14 days, respectively. Subsequently, the impedance modulus experiences a notable increase, reaching $7.28 \times 10^4 \Omega \cdot cm^2$ after immersion for 40 days. This increase is attributed to the formation of a dense protective film of corrosion products on the surface of the metal substrate. The impedance modulus of the samples with vinylic resin (ZRC-M) is higher than that of ZRC-C samples, which is due to the barrier properties.

Electrochemical parameters of coating equivalent circuit

To disentangle the complex interplay between coating properties and corrosion processes, adaptable equivalent circuit models **(**Fig. 8 (a, b**))** were utilized to interpret the EIS plots. As previously observed, the Nyquist diagrams exhibited two-time constants. The low-frequency semicircle is attributed to the coating's resistance (Rp) and capacitance (CPEp), reflecting the protective barrier. The high-frequency arc corresponds to the charge transfer resistance (Rct) associated with the corrosion reaction and the capacitance (CPEdl) of the electric double layer formed on the zinc surface. The constant phase angle indices (α1 and α2) quantify the degree of dispersion effect in each process. General equivalent circuit models for EIS were proposed to fit these results. Model (a) was for all immersion time of ZRC-C and from 48 h to 24 days of ZRC-M and (b) for time between 27 days and 40 days of ZRC-M. This equivalent circuit model represent:

A span of constant phase element of pore (CPEp) and resistance Rp in parallel replaces the dielectric properties of the coating.

A pair of CPE_{dl} (the double layer capacitance) and R_{ct} (the charge transfer resistance) in parallel was adopted to describe the charge transfer process at coating/steel interface of pinholes. Besides, the CPE_{dl} can be used to estimate the quantity of disbonded area between coating and substrate[46].

Warburg (W) impedance is an appropriate diffusion element to describe this as a semi-infinite length diffusion[47] and Rs is the solution resistance.

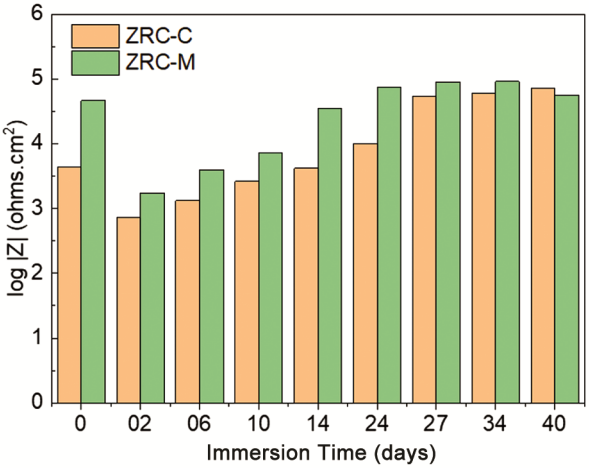

Fig. 7 — Variations of impedance at 10 mHzvs immersion time in 3.5 % NaCl of the zinc-rich paints obtained from Bode plots

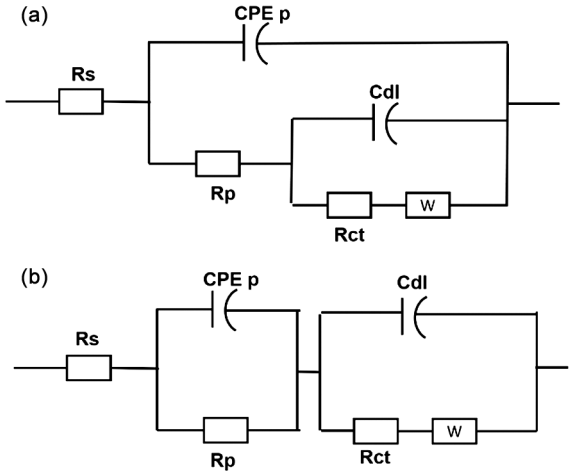

Fig. 8 — Electrical equivalent circuit models used for simulation of the impedance spectra of (a) ZRC-C and ZRC-M at the beginning of immersion and (b) ZRE-M after 24 days of immersion

Constant phase element (CPE) is used as a substitute for the capacitor due to the dispersing effect. For the blocking electrode CPE can be expressed as (Brug *et al.*[49]):

$$CPE = \frac{1}{Q(jw)^{\alpha}} \quad \ldots (4)$$

The parameters α and Q are independent of frequency. When α = 1, Q has units of a capacitance, i.e., F/cm^2, and represents the capacity of the interface. When α ≠ 1, Q has units of sa/Ω.cm^2 (Ref.48) Figs 9 and 10 present the fitted curves for the ZRC-C and ZRC-M coatings. The results demonstrate that the equivalent circuit effectively reproduces the measured EIS data, particularly capturing the capacitive reactance characteristics at high and medium frequencies.

Fig. 11 shows the equivalent circuit element Rp and Rct during 40 days. There's a difference between ZRC-C and ZRC-M. Rp of coatings increases with time, this may attribute to the corrosion products which fill the micro-holes in the coating. The corrosion products of the zinc particles result in a loss of electrical connection between zinc powder and increase the micropore resistance. Furthermore, this suggests that the coating's conductivity is influenced not only by the electrolyte solution within the micropores, but also by the resin itself, as evidenced by the Rp values of ZRC-M. The presence of vinyl appears to increase the coating's resistance after immersion, potentially due to the decease of pore resistance.

Rt of ZRC-M is much lower than that of ZRC-C after immersion time. Based on the OCP analysis, ZRC-C maintains a longer period of cathodic protection than ZRC-M for a better conductive network. The presence of vinyl in ZRC-M promotes the electrical connection between the separated and permeated zinc particles and increases the effective zinc content after immersion time. The value of Rt increases with time. This is because of the decrease of zinc powder and the increase of the corrosion products which fill in the micropores and decrease the electronical connection between zinc particles and steel substrates. The fitted corrosion parameters are presented in Table 4, ZRC-M shows a lower double layer capacitance than ZRC-C. One possible explanation can be associated to the presence of vinyl increase the contact impedance between zinc particles.

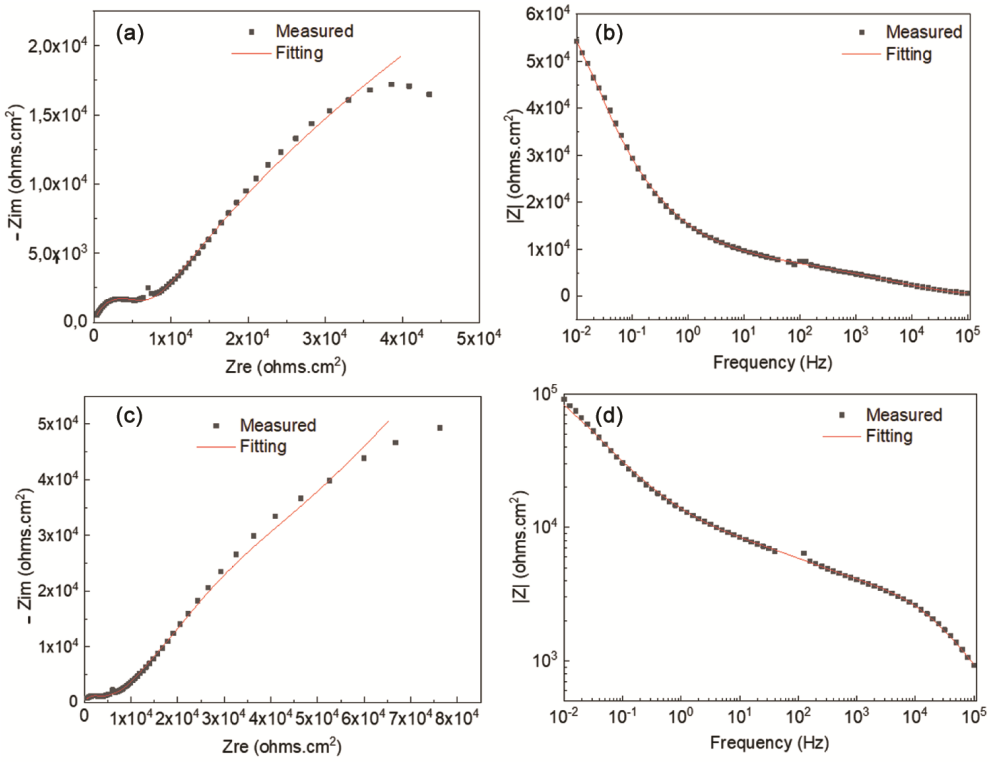

Fig. 9 — EIS and fitting results of the studied coatings: (a1, a2) Bode and Nyquist diagram of ZRC-C and (a3, a4) Bode and Nyquist diagram of ZRC-M after immersion of 27 days

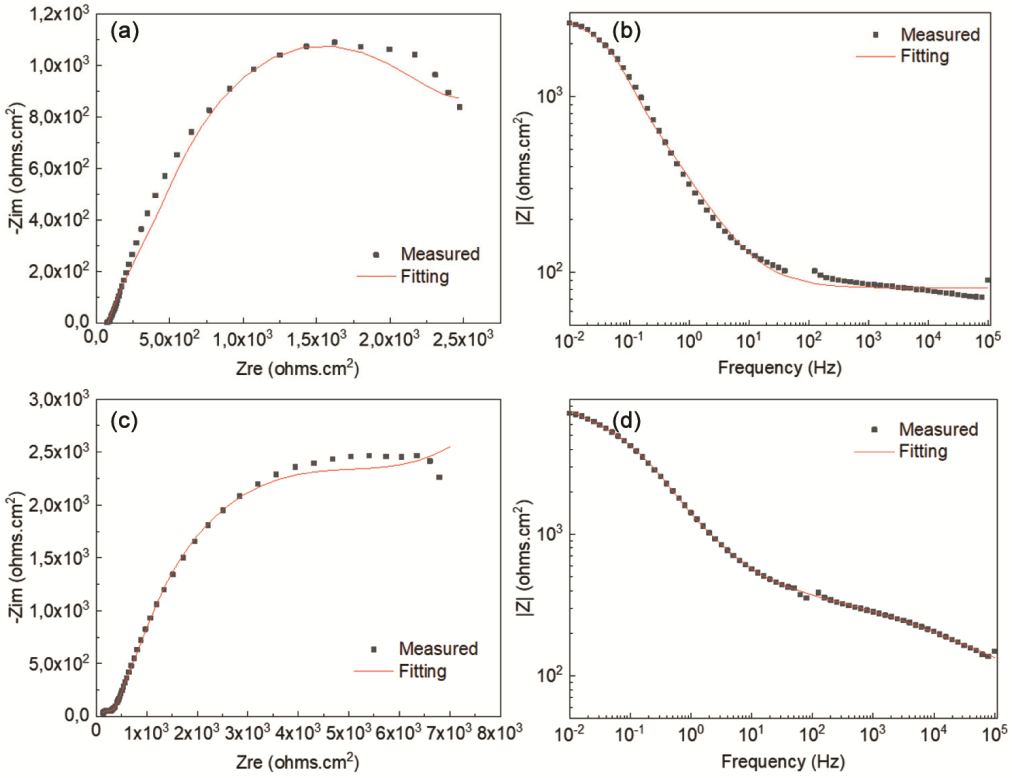

Fig. 10 — EIS and fitting results of the studied coatings:(b1, b3) Bode and Nyquist diagram of ZRC-C and (b3, b4) Bode and Nyquist diagram of ZRC-M after immersion of 10 days

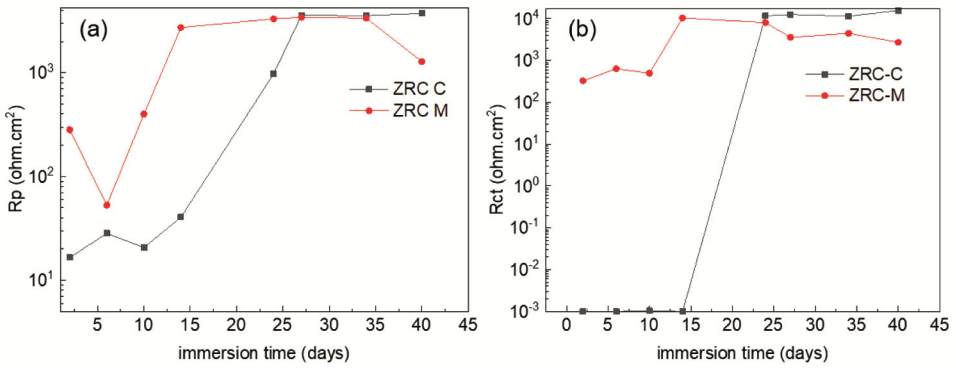

Fig. 11 — Equivalent circuit element (a) Rp and (b) Rct at different immersion time in 3.5 wt% NaCl solution during 40 days

Table 4 — Fitted corrosion parameters of the coatings at different immersion time

Immersion time (days)	Qp (F/cm^2)		α1		Qdl (F/cm^2)		α2	
	ZRC-C	ZRC-M	ZRC-C	ZRC-M	ZRC-C	ZRC-M	ZRC-C	ZRC-M
02	10^{-4}	10^{-4}	0,63	0,48	10^{-4}	10^{-4}	0,76	0,72
06	10^{-4}	10^{-4}	0,64	0,29	10^{-4}	9,99 10^{-5}	0,92	0,41
10	10^{-4}	10^{-4}	0,80	0,34	10^{-4}	9,35 10^{-5}	0.99	0,75
14	10^{-4}	3,91 10^{-5}	0,83	0,59	10^{-4}	3,91 10^{-5}	0,99	0,29
24	1,57 10^{-7}	10^{-7}	0,69	0,69	3,14 10^{-5}	1,64 10^{-5}	0,31	0,43
27	1,01 10^{-7}	8,69 10^{-7}	0,72	0,64	2,79 10^{-5}	1,37 10^{-6}	0,30	0,66
34	1,01 10^{-7}	5,81 10^{-6}	0,70	0,55	2,14 10^{-5}	10^{-7}	0,23	0,68
40	1,28 10^{-7}	3,23 10^{-6}	0,67	0,59	2,49 10^{-5}	6,68 10^{-6}	0,30	0,68

Table 5 — Electrochemical parameters (from Tafel plots)

Samples	E_{corr} (V vs SCE)	I_{corr} µA/cm^2	βa	Bc	R_{po} KΩ.cm^2
ZRC-C	-1,073	0.8097	0,05135236	0,05221741	13.891
ZRC-M	-1,049	1.900	0,05489468	0,0812876	7.488
ZRC-C after IMM 40 days	-0,972	0.065	0,06468096	0,07085364	225.535
ZRC-M after IMM 40 days	-0,915	0,062	0,07059106	0,06495531	236.914

DC linear polarization

The electrochemical parameters such as corrosion potential E_{corr}, corrosion current density I_{corr}, and anodic and cathodicTafel slopes (βa and βc) obtained via Tafel extrapolation method, as well as polarization resistance R_{po}, are listed in Table 5. The R_{po} was evaluated according to the Sterne Geary equation[50].

$$R_{po} = \frac{\beta_a \beta_b}{2.303 I_{corr}(\beta_a + \beta_b)} \quad \ldots (5)$$

Fig. 12 presents the potentiodynamic polarization curves of steels coated with ZRC-M and ZRC-C before and after 40 days of immersion. The addition of vinyl resin noticeably shifts the polarization curves of ZRC-M to more positive values compared to the ZRC-C. Notably, even after immersion, ZRC-M exhibits a more positive corrosion potential (E_{corr}) and a lower corrosion current density (i_{corr}), indicating superior corrosion resistance. This is further corroborated by the higher Rp value of ZRC-M after immersion compared to other coatings. Moreover, the higher β_a values observed for ZRC-M confirm the effective inhibition of the anodic reaction by the vinyl resin.

In the raw state, the incorporation of vinyl leads to a decrease in the coatings' polarization resistance (R_{po}), suggesting that 80% of the zinc powder starts reacting under its influence. However, a significant change occurs in the Tafel plot upon the addition of 2.22 wt% vinyl. distinctly, the corrosion potential of both ZRC-C and ZRC-M samples remains stable at -1.073 V and -1.049 V (vs. SCE), respectively, while the Fe oxidation electrode sits at -0.64 V (vs. SCE). This disparity satisfies the conditions for sacrificial anode cathodic protection.

Morphology of coating after immersion

The surface morphology of the zinc rich coatings was studied after 40 days immersion times and are shown in Fig. 13. The zinc oxides were formed on the surface of the coatings after immersion times. As can be seen in Fig. 13, an impact zinc oxide layer was formed on the surface of ZRC-C and ZRC-M after immersion time. The most of zinc particles were converted to the form of zinc oxide. The surface

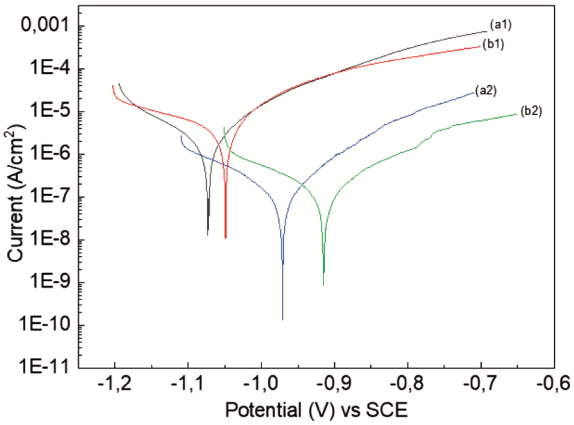

Fig. 12 — Tafel plots of ZRC-C (a1, b1) and ZRC-M (a2, b2) before (a) and after (b) immersion time measured in 3.5 wt% NaCl solution

porosities of the coating reduced significantly after immersion time. This finding demonstrates that barrier properties of were enhanced after 40 days exposure. As a result, the coating could protect metal substrate against corrosion through a barrier mechanism. This can be also responsible for the decrease in coating sacrificial behavior after 40 days.

EDS analysis was performed before and after exposure to the electrolyte and results are given in Fig. 14. An increase in oxygen content and a decrease in zinc content were observed in the ZRC samples. As the exposure duration increased, more oxidation products accumulated on the coating surface. Consequently, due to the elevated oxygen content, zinc have been partially consumed, leading to the formation of zinc oxides. This resulted in a lower zinc content for both the standard zinc-rich coating (ZRC-C) and the modified ones (ZRC-M) after exposure to a 3.5% electrolyte compared to the initial exposure period. It is worth noting that the highest oxygen content, approximately 48.58% by weight, was observed for ZRC-M.

Salt spray test

The corrosion resistance of ZRC was evaluated through salt spray test. As shown in Fig. 15, the photos of different coatings before and after 1110 h of salt spray test have different morphologies. ZRC-C and ZRC-M exhibit varying degrees of spalling as

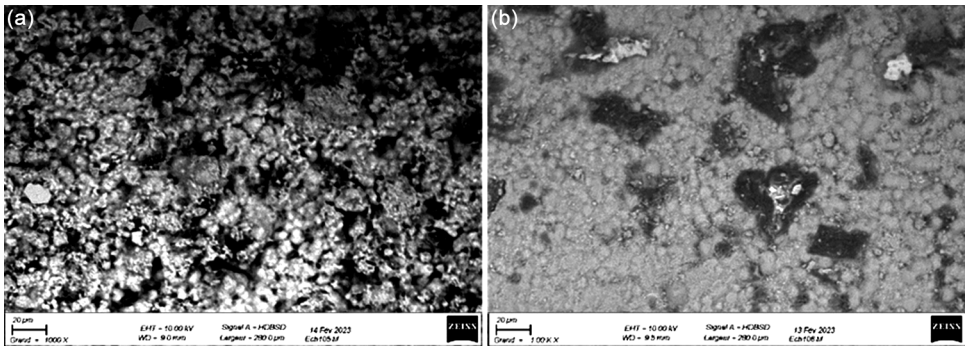

Fig. 13 — SEM micrographs of zinc rich paints (a) ZRC-C and (b) ZRC-M after 40 days immersion time

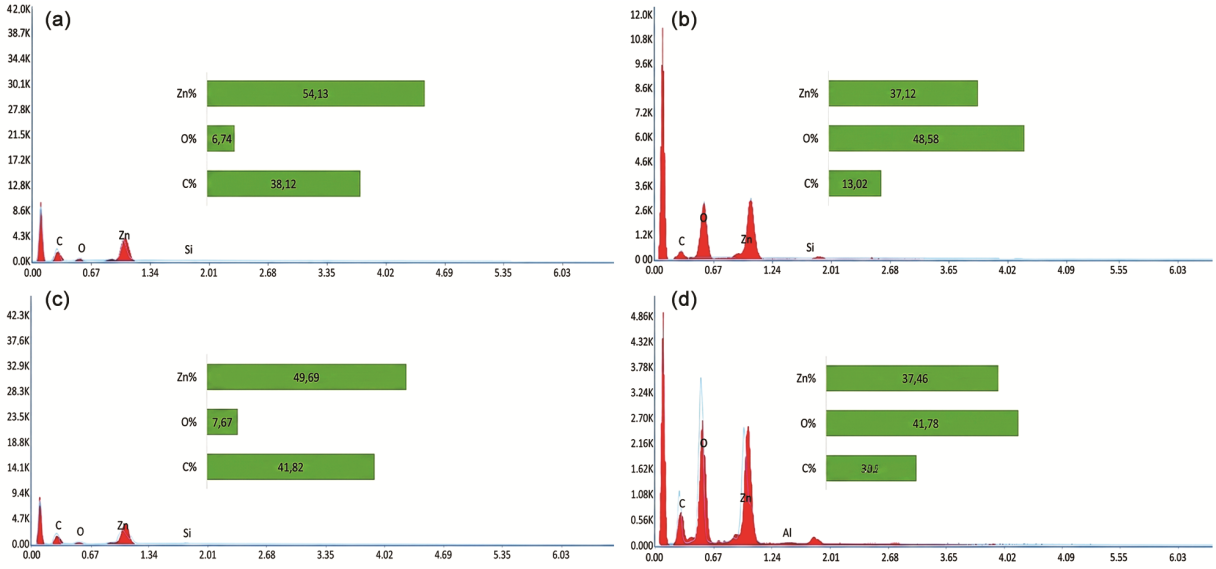

Fig. 14 — EDS of coating before and after immersion time (a1,a2) ZRC-C and (b1,b2) ZRC-M

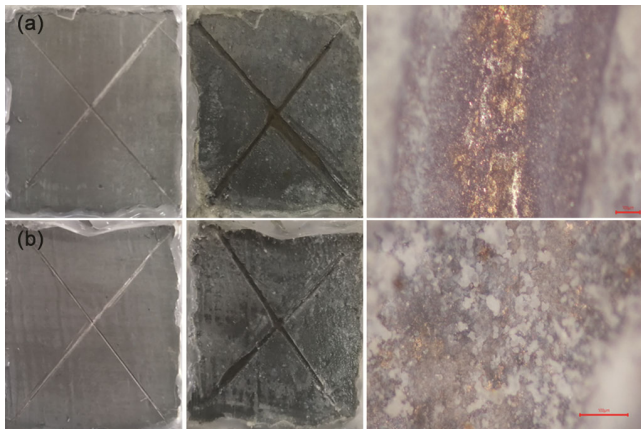

Fig. 15 — Salt spray test results of ZRC-C and ZRC-M coatings respectively (a1, b1) before and (a2, b2) after immersed in salt spray chamber for 1110 h, (a3, b3) the microscopic image on the scribe line

well as the presence of red and yellow rust on and around the score line due to corrosion of the steel and the sacrificial effect of zinc particles, respectively[46]. Further compare the anti-corrosion properties of the coatings. In the final stage of the salt spray test (1110 h), rust spots appeared on the exposed metal surfaces (marking lines) of all coated surfaces. Among them, more than a quarter of ZRC-C's surface is covered with rust spots such as corrosion products, while ZRC-M's density is lower. After 1110 h, white rust appeared more obviously, when the ZRC-M coating was formed, indicating that the coating can protect the metal substrate through a sacrificial mechanism. Less red rust forms inside the cracks compared to ZRC-C.

Conclusion

In summary, the incorporation of vinyl resin significantly improves the corrosion protection performance of zinc-rich coatings on A283 steel. SEM observations confirmed a uniform distribution of zinc particles, while FTIR analysis indicated chemical modification through the formation of C=O groups. Adhesion tests showed that ZRC-M exhibits the highest adhesion strength (9.00 MPa), attributed to

enhanced mechanical interlocking and chemical bonding.

Electrochemical results revealed that ZRC-C provides prolonged sacrificial protection, whereas ZRC-M ensures effective barrier performance by reducing ion permeability through more tortuous diffusion paths. OCP measurements further confirmed that the addition of vinyl resin maintains the sacrificial behavior of zinc. Finally, salt spray tests demonstrated reduced blistering and red rust formation after 1110 h, confirming the improved durability of the modified coatings.

Acknowledgments

The authors would like to thank the Military Polytechnic School for providing the financial support.

Conflict of Interest

The authors declare no conflict of interests.

Reference

1 Rouw A C, Model epoxy powder coatings and their adhesion to steel, *Prog Org Coat*, 34 (1998) 181.
2 Ifran M H, Chemistry and technology of thermosetting polymers in construction applications, Springer, (1998).
3 Tadashi A, Mitsukazu O & Kohichi H, Structure and adhesive properties of epoxy resins modifiedwith core/shell acrylic particles, *J Adhes Sci Technol*, 12 (1998) 749.
4 Rudawskaa A & Czarnot M, Selected aspects of epoxy adhesive compositions curing process, *J Adhes Sci Technol*, 27 (2013) 1933.
5 Schaefer K & Miszczyk A, Improvement of electrochemical action of zinc-rich paints by addition of nanoparticulate zinc, *Corros Sci*, 66 (2013) 380.
6 Marchebois H, Savall C, Bernard J & Touzain S, Electrochemical behavior of zinc-rich powder coatings in artificial sea water, *Electrochim Acta*, 49 (2004) 2945.
7 Zeng D F, Tao N W, Jiang S W & Wang J N, NORSOK M-501 test method for heavy-duty anticorrosive marine coatings, *Coat Ind*, 45 (2015) 51.
8 Cheng L, Luo Y, Ma S, Guo W & Wang X, Corrosion resistance of inorganic zinc rich coating reinforced by Ni-coated coal fly ash, *J Alloys Compd*, 786 (2019) 791.
9 Munger C G & Vincent L D, Corrosion prevention by protective coatings, Edn 2nd, NACE, (1999).
10 Kalendova A, Effects of particle sizes and shapes of zinc metal on the properties of anticorrosive coatings, *Prog Org Coat*, 46 (2003) 324.
11 Isomina A S & Savronov A P, Effect of interphase interaction within zinc-filled composite coating on the potential of cathodic protection of steel, *Russ J Phys Chem A*, 85 (2011) 2227.
12 Armelin E, Marti M, Liesa F, Iribarren J I & Aleman C, Partial replacement of metallic zinc dust in heavy duty protective coatings by conducting polymer, *Prog Org Coat*, 69 (2010) 26.
13 Akbarinezhad E, Ebrahimi M, Sharif F & Ghanbarzadeh A, Evaluating protection performance of zinc rich epoxy paints modified with polyaniline and polyaniline-clay nanocomposite, *Prog Org Coat*, 77 (2014) 1299.
14 Suherman H, Sahari J & Sulong A B, Effect of small-sized conductive filler on the properties of an epoxy composite for a bipolar plate in a PEMFC, *Ceram Int*, 39 (2013) 7159.
15 Park S M & Shon M Y, Effects of multi-walled carbon nano tubes on corrosion protection of zinc rich epoxy resin coating, *J Ind Eng Chem*, 5 (2014) 42.
16 Gergely A, Pászti Z, Mihály J, Drotár E & Török T, Galvanic function of zinc-rich coatings facilitated by percolating structure of the carbon nanotubes Part II: Protection properties and mechanism of the hybrid coatings, *Prog Org Coat*, 77 (2014) 412.
17 Arman S Y, Ramezanzadeh B, Farghadani S, Mehdipour M & Rajabi A, Application of the electrochemical noise to investigate the corrosion resistance of an epoxy zinc-rich coating loaded with lamellar aluminum and micaceous iron oxide particles, *Corros Sci*, 77 (2013) 118.
18 Kakaei M N, Danaee I & Zaarei D, Investigation of corrosion protection afforded by inorganic anticorrosive coatings comprising micaceous iron oxide and zinc dust, *Corros Eng Sci Technol*, 48 (2013) 194.
19 Jagtap R N, Patil P P & Hassan S Z, Effect of zinc oxide in combating corrosion in zinc-rich primer, *J Prog Org Coat*, 63 (2008) 389.
20 Gergely A, Pfeifer É, Bertóti I, Török T & Kálmán E, Corrosion protection of cold-rolled steel by zinc-rich epoxy paint coatings loaded with nano-size alumina supported polypyrrole, *Corros Sci*, 53 (2011) 3486.
21 Shirehjini F T, Danaee I, Eskandari H & Zarei D, Effect of nano clay on corrosion protection of zinc-rich epoxy coatings on steel 37, *Mater Sci Technol*, 32 (2016) 1152.
22 Hussain A K, Seetharamaiah N, Pichumani M & Chakra C S, Research progress in organic zinc rich primer coatings for cathodic protection of metals-A comprehensive review, *Prog Org Coat*, 153 (2021) 106040.
23 Zhang X, Rajaraman B R, Liu H & Ramakrishna S, Graphene's potential in materials science and engineering, *RSC Adv*, 4 (2014) 28987.
24 Dhongde N R, Adhikari S & Rajaraman P V, Anticorrosion properties of ionic liquid functionalized graphene oxide epoxy composite coating on the carbon steel for CCUS environment, *Environ Sci Pollut Res*, 32 (2025) 4511.
25 Zhou S, Wu Y, Zhao W, Yu J, Jiang F, Wu Y & Ma L, Designing reduced graphene oxide/zinc rich epoxy composite coatings for improving the anticorrosion performance of carbon steel substrate, *Mater Des*, 169 (2019) 107694.
26 Ramezanzadeh B, Moghadam M M H, Shohani N & Mahdavian M, Effects of highly cystalline and conductive polyaniline/graphene oxide composites on the corrosion protection performance of a zinc-rich epoxy coating, *Chem Eng J*, 320 (2017) 363.
27 Teng S, Gao Y, Cao F, Kong D, Zheng X, Ma X & Zhi L, Zinc-reduced graphene oxide for enhanced corrosion protection of zinc-rich epoxy coatings, *Prog Org Coat*, 123 (2018) 185.
28 Parhizkar N, Shahrabi T & Ramezanzadeh B, A new approach for enhancement of the corrosion protection properties and interfacial adhesion bonds between the epoxy coating and steel substrate through surface treatment by covalently modified amino functionalized graphene oxide film, *Corros Saf*, 123 (2017) 55.
29 Shen L, Zhao W, Wang K & Xu J, GO-Ti_3C_2 two-dimensional heterojunction nanomaterial for anticorrosion

enhancement of epoxy zinc-rich coatings, *J Hazard Mater*, 417 (2021) 126048.
30 Tian Y, Bi Z & Cui G, Study on the corrosion resistance of graphene oxide-based epoxy zinc-rich coatings, *Polymers*, 13 (2021) 1657.
31 Bastos A, Zheludkevich M & Ferreira M, A SVET investigation on the modification of zinc dust reactivity, *Prog Org Coat*, 63 (2008) 282.
32 Park J H, Yun T H, Kim K Y, Song Y K & Park J M, The improvement of anticorrosion properties of zinc-rich organic coating by incorporating surface-modified zinc particle, *Prog Org Coat*, 74 (2012) 25.
33 Wang J, Qi Y, Zhao X & Zhang Z, Electrochemical investigation of corrosion behavior of epoxy modified silicate zinc-rich coatings in 35% NaCl solution, *Coatings*, 10 (2020) 444.
34 Ding R, Chen S, Lv J, Zhang W, Zhao X D, Liu J, Wang X, Gui T J, Li B J & Tang Y Z, Study on graphene modified organic anti-corrosion coatings: A comprehensive review, *J Alloys Compd*, 806 (2019) 611.
35 Shi X, Nguyen T A, Suo Z & Liu Y & Avci R, Effect of nanoparticles on the anticorrosion and mechanical properties of epoxy coating, *Surf Coat Technol*, 204 (2009) 237.
36 Langer E, Zubielewicz M, Kuczy´nska H, Kr´olikowska A & Komorowski L, Anticorrosive effectiveness of coatings with reduced content of Zn pigments in comparison with zinc-rich primers, *Corros Eng Sci Technol*, 54 (2019) 627.
37 Buchheit R G, Corrosion resistant coating and paints, handbook of environmental degradation of materials (Edn 2nd), (2012).
38 Bentley J, Organic film formers, paint and surface coating (Edn 2nd), (1999).
39 Duval S, Keddam M, Sfaira M, Srhiri A & Takenouti H, Electrochemical impedance spectroscopy of epoxy-vinyl coating in aqueous medium analyzed by dipolar relaxation of polymer, *J Electrochem Soc*, 149 (2002) B520.
40 Nandiyanto A B D, Oktiani R & Ragadhita R, How to read and interpret FTIR spectroscope of organic material, *Indones J Sci Technol*, 4 (2019) 97.
41 Dhongde N R, Baranwal P K & Rajaraman P V, Functionalization of graphene oxide with an ionic liquid (1-butyl-3-methylimidazolium acetate): Preparation of epoxy-based coating on carbon steel for anticorrosive applications, *J Appl Polym Sci*, 140 (2023).
42 Dhongde N R, Das N K, Hazarika J, Park J G, Banerjee T & Rajaraman P V, Azoles as corrosion inhibitors in alkaline medium for ruthenium chemical mechanical planarization applications: Electrochemical and theoretical analysis, *J Mol Struct*, 1320 (2025) 139651.
43 Suherman H, Sahari J & Sulong A B, Effect of small-sized conductive filler on the properties of an epoxy composite for a bipolar plate in a PEMFC, *Ceram Int*, 39 (2013) 7159.
44 Cheng L, Liu C, Han D, Ma S, Guo W, Cai H & Wang X, Effect of graphene on corrosion resistance of waterborne inorganic zinc-rich coatings, *J Alloys Comp*, 774 (2019) 255.
45 Pethrick R A, Hollins E A, McEwan L, Pollock A, Hayward D & Johncock P, Effect of cure temperature on the structure and water absorption of epoxy/amine thermosets, *Polym Int*, 39 (1996) 275.
46 Naderi R, Attar M M & Moayed M H, EIS examination of mill scales on mild steel with polyester-epoxy powder coating, *Prog Org Coat*, 50 (2004) 162.
47 Li H Y, Duan J Y & Wei D D, Comparison on corrosion behaviour of arc sprayed and zinc-rich coatings, *Surf Coat Technol*, 235 (2013) 259.
48 Orazem M E & Tribollet B, Electrochemical impedance spectroscopy, Wiley Edn (2008).
49 Meroufel A & Touzain S, EIS characterisation of new zinc-rich powder coatings, *Prog Org Coat*, 59 (2007) 197.
50 Arianpouya N, Shishesaz M, Arianpouya M & Nematollahi M, Evaluation of synergistic effect of nanozinc/nanoclay additives on the corrosion performance of zinc-rich polyurethane nanocomposite coatings using electrochemical properties and salt spray testing, *Surf Coat Technol*, 216 (2013) 199.